

Modeling, Analysis and Testing of a Novel Spoke-Type Interior Permanent Magnet Motor with Improved Flux Weakening Capability

Alberto Tassarolo, Mario Mezzarobba and Roberto Menis

Engineering and Architecture Department, University of Trieste, 34127 Trieste, Italy

Spoke-type interior permanent magnet (IPM) machines are an attractive topology for high performance electric motors, especially designed for vehicle traction applications. In this paper, a special design for a spoke-type IPM motor is presented to enhance motor flux-weakening capability in the operation over a wide speed range. The proposed design consists of a simple and robust mechanical device that includes radially-displaceable rotor yokes, connected to the shaft by means of springs. At high speed, the centrifugal force prevails over the elastic one due to springs, causing the mobile yokes to displace radially and to establish a partial magnetic short circuit between permanent magnets. This increases permanent magnet leakage flux and consequently reduces the air-gap field. As a result, a mechanical flux weakening effect is achieved at high speed, which helps significantly reduce the demagnetizing d -axis current to be injected by the inverter, along with the related copper losses and demagnetization issues. The proposed design is investigated in the paper using an analytical model whose parameters are computed by finite-element analysis (FEA). The effectiveness of the solution being set forth is successfully proven by some testing on a laboratory prototype. Experimental results are compared to analytical predictions showing a satisfactory accordance.

Index Terms—Flux weakening, interior permanent magnet motors, spoke-type permanent magnet machines vehicle traction drives.

I. INTRODUCTION

IN many applications, such as spindle drives [1], household appliances [2], automotive propulsion [3]-[5] and power generation [8], large use is made of permanent magnet (PM) synchronous motors and generators designed to operate over a wide speed range. In these applications, in order not to exceed the voltage capabilities of motor-connected power electronics equipment, permanent magnet flux is to be weakened when the speed grows above a certain value, usually referred to as base speed. Normally, the flux weakening is performed by injecting a demagnetization stator current along the d axis [7]-[9], which can be critical for different reasons: firstly, it leads to an increase in converter rating [8]; secondly, it causes poor efficiency values at high speed due to large copper losses and limits the available current margin for torque production [9]; thirdly, it may lead to possible rotor demagnetization issues [7] due to high armature reaction field.

In order to extend the speed range of PM machines while limiting converter ratings and motor losses at high speeds, several authors have tried to act on rotor electromagnetic and/or mechanical design [10], [11]. To quote some examples, centrifugal force at high speeds is exploited in [12] to force mobile interior permanent magnets into a new position where they produce lower air-gap flux due to an increased reluctance path. In [13] the flux weakening is also achieved through an appropriate displacement of mobile permanent magnets, but using magneto-restrictive material properties instead of centrifugal force. In [5] the air-gap at high speeds is reduced by means of an axial shaft displacement so as to reduce the effective rotor core length. Moreover, in some other designs circular-shaped permanent magnets are proposed and their rotation is used to adjust air-gap flux depending on the speed [11]. Finally, in [14], [15] designs are proposed encompassing movable ferromagnetic elements embedded in the flux barriers of interior permanent magnet (IPM) machines in order to suitably adjust permanent magnet flux leakage and, hence, the flux weakening performance of the motor.

In this paper, a novel rotor mechanical design for flux weakening performance improvement is proposed applying to interior permanent magnet (IPM) machines with spoke-type magnet arrangement [2], [7], [13], [16]-[18]. Spoke-type IPM motors have been extensively considered over recent years in both conventional [2], [7] and modified [12], [13], [16]-[18] arrangements thanks to their high flux density potential. This makes them especially suitable for automotive applications [3], [7], [12], [13] and for reducing the use of rare earth materials [18] in favor of cheaper ferrite magnets [7].

The design modification herein proposed to spoke-type IPM motors consists of equipping the usual machine topology with a self-activating mechanical device which, depending on the speed, establishes or removes a partial magnetic short circuit between adjacent spoke-arranged permanent magnets, so as to decrease or increase the rotor flux portion that crosses machine air-gap [19]. The device activates automatically by centrifugal force when the speed exceeds a given threshold and deactivate on return to low speed operation. Compared to previous flux weakening methods acting on IPM rotor design, the proposed solution appears very simple and robust from a construction and operation viewpoint and requires minimal room consumption for flux weakening device installation.

After briefly describing the proposed design arrangement, its operation is investigated in the paper through an analytical non-linear model taking magnetic saturation effects into account. Efficient methods to determine model parameters are presented based on a limited set of finite-element analysis (FEA) magneto-static simulations. Finally, the new IPM motor performance is experimentally assessed in terms of flux weakening capabilities by testing on a laboratory prototype. Tests are presented both at no load and in loaded conditions, showing the effectiveness of the solution being set forth as well as a satisfactory matching between experimental data and theoretical predictions obtained from the proposed mathematical model.

II. MOTOR MECHANICAL DESIGN DESCRIPTION

The proposed spoke-type IPM motor features a conventional three-phase stator and an innovative mechanical rotor design which is illustrated in Fig. 1.

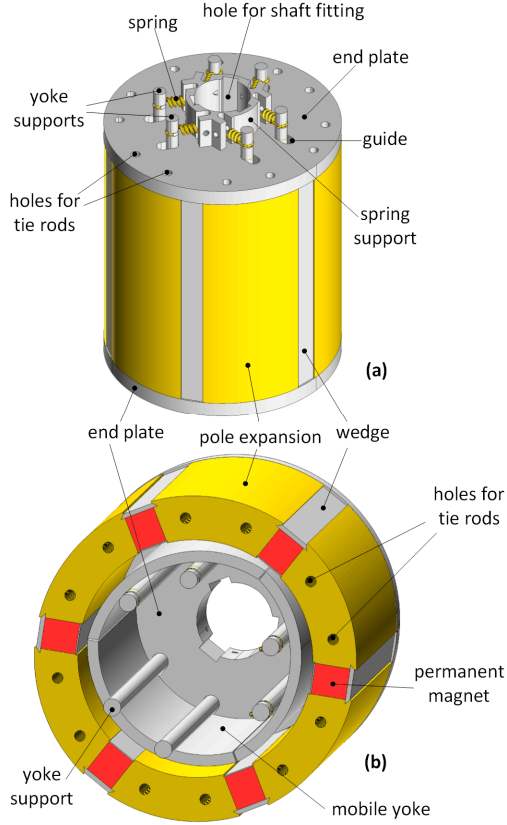


Fig. 1. (a) External motor view; (b) motor cross section at half core length.

The main modification with respect to the conventional spoke-type rotor arrangement [2], [7] consists of a set of ferromagnetic arc-shaped mobile yokes placed between pole expansions and the shaft (Fig. 1b) and capable of sliding in the radial direction to achieve flux weakening effects as discussed in the next Section.

End plates are used to fix rotor poles to the shaft leaving the necessary space between it and rotor active parts to accommodate mobile yokes. So, rotor poles and permanent magnets are mechanically connected to the shaft, as depicted in Fig. 1, by means of end plates. These are provided with holes for the insertion of bolted tie rods, whose function is to give the rotor structure the needed axial compactness. Tie rods are also needed to secure rotor poles in the radial direction counteracting centrifugal stresses. End plates are fixed to the shaft by keys and need be dimensioned considering that they transfer all the torque from rotor active parts to the shaft. For their construction, a non-magnetic stainless steel material is used in order to limit flux leakage at rotor core ends.

Permanent magnets are fixed to rotor poles by means of two non-magnetic wedges: an upper (thicker) wedge dimensioned to withstand centrifugal forces and a lower (thinner) wedge used to support permanent magnets when the rotor is at standstill or at very low speeds.

The use of end plates for torque transmission allows for mobile yokes to be accommodated between the internal surface of pole expansions and the external surface of the shaft. Each mobile yoke is equipped with two axial supports welded to it (Fig. 1b) and connected to end-plate overhangs by means of springs. When springs extend under centrifugal force effect, mobile yokes can displace radially as their supports slide through suitable guides drilled in the end plates.

The physical implementation of the rotor design described above into a laboratory prototype is illustrated in Fig. 2 and Fig. 3. As regards the stator part, it is conventional as shown in Fig. 4.

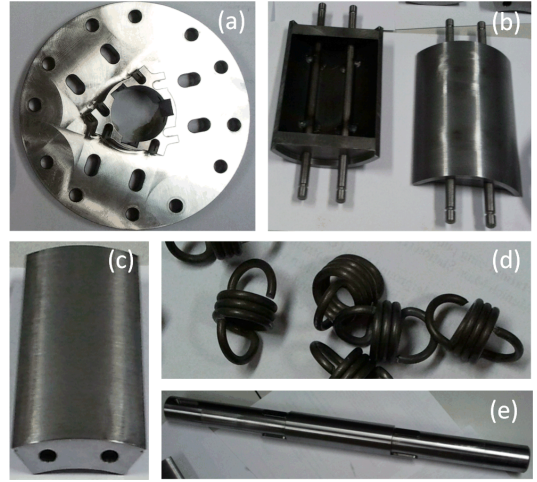


Fig. 2. Prototype rotor components: (a) end plates; (b) mobile yokes; (c) pole expansions; (d) springs; (e) shaft.

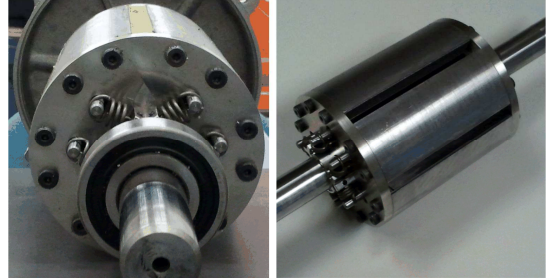


Fig. 3. Assembled rotor of machine prototype.

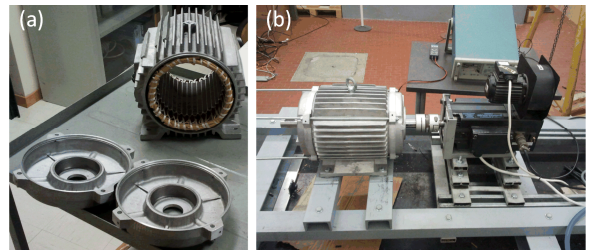


Fig. 4. (a) Prototype machine stator; (b) prototype motor on the test bench.

The ratings of the prototype machine are provided in Table I. Its characteristic dimensions, according to the nomenclature defined in Fig. 5, are given in Table II. Finally, the main electrical data for stator design are provided in Table III.

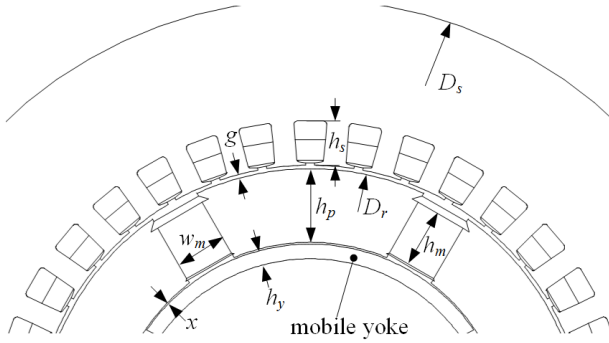


Fig. 5. Symbols used to define prototype motor dimensions.

TABLE I
MAIN RATINGS OF THE IPM MOTOR PROTOTYPE

Base frequency	50 Hz
Base speed	1000 rpm
Maximum speed	2500 rpm
Base voltage	340 V
Base torque	15 Nm
Phase current	8 A

TABLE II
DIMENSIONS OF THE PROTOTYPE IPM MOTOR PROTOTYPE

Stator outer diameter, D_s	240 mm
Rotor outer diameter, D_r	148 mm
Stator slot height, h_s	12 mm
Rotor pole height, h_p	20 mm
Permanent magnet height, h_m	15.8 mm
Permanent magnet width, w_m	14 mm
Air-gap width, g	1 mm
Mobile yoke thickness, h_y	4 mm
Minimum gap x between yoke and rotor	0 mm
Maximum gap x between yoke and rotor	5 mm
Core length, L	150 mm

TABLE III
WINDING DATA OF THE IPM MOTOR

Number poles	6
Number of stator slots	36
Number of stator phases	3
Number of winding layers	2
Coil to pole pitch ratio	5/6
Number of turns per coil	21
Number of series-connected turns per phase	252
Phase resistance, r (Ω)	2.93

III. MOTOR PRINCIPLE OF OPERATION

The operating principle of the proposed IPM motor can be summarized as shown in Fig. 6.

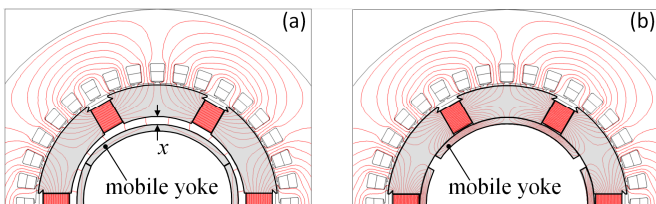


Fig. 6. Proposed IPM motor configuration (a) at low speed; (b) at high speed

In qualitative terms, when the machine rotates at low speed, the elastic force exerted by springs retains mobile yokes close to the shaft, so that a certain gap of width x (Fig. 6a) exists between them and the inner rotor rim. In these conditions, practically all permanent magnet flux flows through the air-gap into the stator and the machine operates as a normal spoke-type IPM motor.

At higher speeds, the centrifugal force acting on mobile yokes increases and prevails over the retaining force exerted by the springs. The latter then extend and the mobile yokes translate radially into a new position (Fig. 6b) where they practically touch the inner surface of rotor pole expansions. In these conditions, it is clear that part of permanent magnet flux is drained into the mobile yokes. This causes a significant increase in permanent magnet leakage field and, consequently, a reduction in the no-load air-gap flux. In other words, a spontaneous flux weakening occurs, as illustrated in Fig. 7 which shows the no-load air-gap flux density profile over a double pole span when for the two extreme positions of mobile yokes as resulting from a magneto-static FEA simulation.

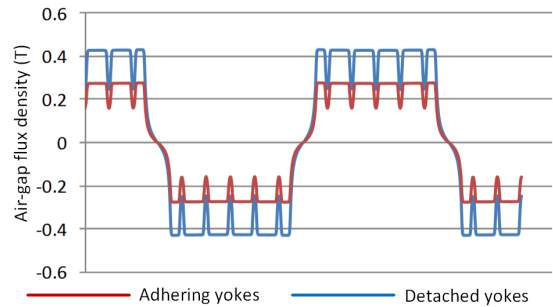


Fig. 7. No-load air-gap flux density for the two extreme yoke positions.

If mobile yokes were infinitely permeable, all permanent magnet flux would flow through them at high speeds and the air-gap field would then be almost reduced to zero. In practice, yokes have a finite permeability and width h_y (Fig. 6) — the latter limited by the available space between rotor poles and the shaft — and therefore some magnetic saturation inevitably occurs in them. This limits the intrinsic flux weakening capability that the IPM motor can attain through the proposed design modification method.

IV. MOTOR MATHEMATICAL MODELING FOR ELECTROMECHANICAL PERFORMANCE PREDICTION

Although conceptually simple and practically easy to implement from a construction viewpoint, the described IPM motor design poses some major challenges when it comes to predict its performance in its various possible operating conditions, e.g. at different loads and different speeds, hence for different mobile yoke positions.

One difficult arises from the system being strongly non-linear. In fact, at low speed (when the mobile yokes are detached from rotor poles, Fig. 6a), magnetic saturation could be neglected as sometimes done in the literature to simplify the analysis, provided that the machine is designed with relatively low flux density values in the magnetic cores [16]-[18]. Conversely, it becomes impossible to use a linear model

to study machine operation at high speeds (Fig. 6b) due to the strong magnetic saturation occurring in the yokes as discussed in the previous Section.

Furthermore, it is to be noted that mobile yoke motion, in addition to depending on centrifugal force and on the elastic force exerted by springs, is also affected by the magnetic attraction force due to the magnetic field in the gap between the yokes and the rotor pole expansions [19]. Such a force may significantly vary with the operating conditions as the mentioned field flowing through mobile yokes is due to permanent magnets and to stator currents as well.

A further issue relates to the fact that, unlike conventional rotating machines, the proposed IPM motor features a rotor variable geometry depending on mobile yoke instantaneous position. In more rigorous terms, the geometric state of the machine is, at any time, described not only by the angular rotor position, but also by the yoke radial displacement x (Fig. 5). In such sense, the motor should be regarded as a multiple-degrees-of-freedom one. This causes noticeable difficulties if one wants, for example, to model the system in a time-stepping FEA environment [20] in order to study machine transients or to predict mobile yoke dynamic behavior. In fact, most of commercial time-stepping FEA programs allow for motion effects to be accounted for but on condition that they can be described by one single independent variable (which could be the angle around a rotational center or the displacement along a fixed linear direction).

As a result of the above mentioned considerations, the need arises to investigate the performance of the system under study through a sufficiently accurate analytical model where both non-linearity effects due to magnetic saturation and the multiple degrees of freedom in system motion (rotor revolution combined with mobile yoke translation) are suitably taken into account.

Next, the electromechanical model of the machine will be presented first working with physical phase variables and then applying a dq transformation [5].

A. Machine electromagnetic equation in three-phase variables

Calling a , b , c the three stator phases, machine phase voltages, currents and flux linkages are represented by the following vectors:

$$\mathbf{v}_{abc} = \begin{pmatrix} v_a \\ v_b \\ v_c \end{pmatrix}, \mathbf{i}_{abc} = \begin{pmatrix} i_a \\ i_b \\ i_c \end{pmatrix}, \boldsymbol{\lambda}_{abc} = \begin{pmatrix} \lambda_a \\ \lambda_b \\ \lambda_c \end{pmatrix} \quad (1)$$

which are linked by the well-known voltage equation:

$$\mathbf{v}_{abc} = r\mathbf{i}_{abc} + \frac{d\boldsymbol{\lambda}_{abc}}{dt} \quad (2)$$

where r represents phase resistance.

B. Machine electromagnetic equation in dq variables

In order to obtain a compact electromagnetic torque expression and to work with time-invariant variables at steady-state, it is convenient to write machine equations in a rotating dq reference frame attached to the rotor and defined so that the d axis coincides with the no-load flux symmetry

axis. This can be done through the Clarke's and Park's transformations matrices below

$$\mathbf{C} = \sqrt{\frac{2}{3}} \begin{pmatrix} 1 & -\frac{1}{2} & -\frac{1}{2} \\ 0 & -\frac{\sqrt{3}}{2} & \frac{\sqrt{3}}{2} \end{pmatrix}, \mathbf{P}(\theta) = \begin{pmatrix} \cos(\theta) & \sin(\theta) \\ -\sin(\theta) & \cos(\theta) \end{pmatrix} \quad (3)$$

where θ indicates the rotor (d axis) angular position (in electrical radians) with respect to the symmetry axis of stator phase a . Combining \mathbf{C} and \mathbf{P} the overall abc to dq transformation \mathbf{T} is obtained as per (4). It can be easily proved that \mathbf{T} satisfies the

$$\mathbf{T}(\theta) = \mathbf{P}(\theta)\mathbf{C} \quad (4)$$

It can be easily checked that \mathbf{T} satisfy the following equalities:

$$\mathbf{T}(\theta)\mathbf{T}(\theta)^t = \begin{pmatrix} 1 & 0 \\ 0 & 1 \end{pmatrix} \quad (5)$$

$$\mathbf{T}(\theta) \frac{d}{d\theta} [\mathbf{T}(\theta)^t] = \omega \mathbf{J}, \quad \frac{d}{d\theta} [\mathbf{T}(\theta)] \mathbf{T}(\theta)^t = -\omega \mathbf{J} \quad (6)$$

where

$$\mathbf{J} = \begin{pmatrix} 0 & -1 \\ 1 & 0 \end{pmatrix} \quad (7)$$

Applying \mathbf{T} to phase variable vectors (1) yields:

$$\mathbf{v}_{dq} = \begin{pmatrix} v_d \\ v_q \end{pmatrix} = \mathbf{T}(\theta)\mathbf{v}_{abc}, \quad \mathbf{i}_{dq} = \begin{pmatrix} i_d \\ i_q \end{pmatrix} = \mathbf{T}(\theta)\mathbf{i}_{abc}, \quad \boldsymbol{\lambda}_{dq} = \begin{pmatrix} \lambda_d \\ \lambda_q \end{pmatrix} = \mathbf{T}(\theta)\boldsymbol{\lambda}_{abc} \quad (8)$$

Using (4)-(8), the voltage equation (9) transforms into:

$$\mathbf{v}_{dq} = r\mathbf{i}_{dq} + \omega \mathbf{J} \boldsymbol{\lambda}_{dq} + \frac{d}{dt} \boldsymbol{\lambda}_{dq} \quad (9)$$

In general, flux linkages λ_d and λ_q are non-linear functions of currents i_d , i_q but, for the machine under study, they are also affected by the gap x between rotor poles and mobile yokes. In fact, for any given i_d , i_q , the air-gap flux strongly depends on x , as shown by Fig. 7 in the particular case when $i_d=i_q=0$. So we can write:

$$\lambda_d = \lambda_d(i_d, i_q, x), \quad \lambda_q = \lambda_q(i_d, i_q, x) \quad (10)$$

$$\frac{d\lambda_d}{dt} = \frac{\partial \lambda_d}{\partial i_d} \frac{di_d}{dt} + \frac{\partial \lambda_d}{\partial i_q} \frac{di_q}{dt} + \frac{\partial \lambda_d}{\partial x} \frac{dx}{dt} \quad (11)$$

$$\frac{d\lambda_q}{dt} = \frac{\partial \lambda_q}{\partial i_d} \frac{di_d}{dt} + \frac{\partial \lambda_q}{\partial i_q} \frac{di_q}{dt} + \frac{\partial \lambda_q}{\partial x} \frac{dx}{dt} \quad (12)$$

and the derivative of $\boldsymbol{\lambda}_{dq}$ in (9) can be written as:

$$\frac{d}{dt} \boldsymbol{\lambda}_{dq} = \frac{d}{dt} \begin{pmatrix} \lambda_d \\ \lambda_q \end{pmatrix} = \boldsymbol{\Lambda}_I(i_d, i_q, x) \frac{d}{dt} \mathbf{i}_{dq} + \boldsymbol{\Lambda}_x(i_d, i_q, x) \frac{dx}{dt} \quad (13)$$

where

$$\boldsymbol{\Lambda}_I(i_d, i_q, x) = \begin{pmatrix} \delta \lambda_d / \delta i_d & \delta \lambda_d / \delta i_q \\ \delta \lambda_q / \delta i_d & \delta \lambda_q / \delta i_q \end{pmatrix} \quad (14)$$

$$\boldsymbol{\Lambda}_x(i_d, i_q, x) = \begin{pmatrix} \delta \lambda_d / \delta x \\ \delta \lambda_q / \delta x \end{pmatrix} \quad (15)$$

This leads to rewrite (9) as

$$\mathbf{v}_{dq} = r\mathbf{i}_{dq} + \omega \mathbf{J} \boldsymbol{\lambda}_{dq} + \boldsymbol{\Lambda}_I \frac{d}{dt} \mathbf{i}_{dq} + \boldsymbol{\Lambda}_x \frac{dx}{dt} \quad (16)$$

from which the following non-linear differential equations for motor dq current vector \mathbf{i}_{dq} results:

$$\frac{d}{dt} \mathbf{i}_{dq} = \Lambda_I(i_d, i_q, x)^{-1} \left[\mathbf{v}_{dq} - \mathbf{r}_{dq} - \omega \mathbf{J} \Lambda_{dq}(i_d, i_q, x) - \Lambda_x(i_d, i_q, x) \frac{dx}{dt} \right] \quad (17)$$

C. Mechanical equation for rotor angular motion

The dynamics of rotor speed and position is governed by the known mechanical equation:

$$T_m - T_r = J \frac{d^2 \theta}{dt^2} = \frac{J}{p} \frac{d^2 \theta}{dt^2} \quad (18)$$

where T_m is the motor electromagnetic torque, T_r is the load torque, p is the number of pole pairs and J is the overall inertia coefficient of the motor and the coupled rotating equipment.

The electromagnetic torque T_m can be expressed as follows:

$$T_m = p \mathbf{i}_{dq}^t \mathbf{J} \boldsymbol{\lambda}_{dq} = p \left[\lambda_d(i_d, i_q, x) i_q - \lambda_q(i_d, i_q, x) i_d \right] \quad (19)$$

Such expression is known to hold also for saturated permanent magnet electric machines [21].

D. Mechanical equation for rotor yoke radial motion

As regard the dynamics of mobile yoke translation, each yoke is subject to three forces (Fig. 8): the elastic force F_e exerted by the springs; the centrifugal force F_c due to shaft revolution and the magnetic force F_m which originates from the magnetic field between the yoke and the pole expansions.

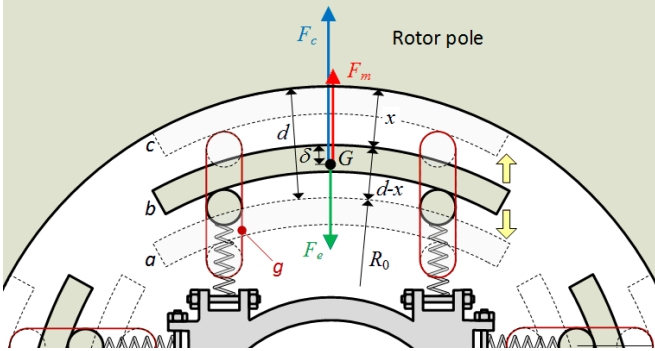


Fig. 8. Ferromagnetic mobile yoke sliding along guides g in: a —rest position (low speed); b —intermediate position during displacement; c —pole-attached position (high speed).

The following differential equation can be thereby written which governs the yoke displacement over time:

$$m \frac{d^2(d-x)}{dt^2} = -m \frac{d^2 x}{dt^2} = F_m + F_c - F_e \quad (20)$$

where m is the yoke mass and d is the maximum gap between the yoke and the rotor pole expansion (Fig. 8).

The centrifugal force depends on the rotor mechanical speed ω_m according to the low:

$$F_c = m \omega_m^2 (R_0 + d - x - \delta) \quad (21)$$

where δ is the minimum distance between the yoke center of gravity and its external surface (Fig. 7) and

$$\omega_m = \frac{1}{p} \frac{d\theta}{dt} \quad (22)$$

Calling k the spring constant, the expression for the elastic force F_e is:

$$F_e = F_{e0} + k(d-x) \quad (23)$$

where F_{e0} indicates the spring “pre-load”, i.e. the elastic force exerted by the spring when the yoke is in its rest position.

Regarding the magnetic force F_m , it depends on the field intensity in the region between the yoke and the pole expansion as well as on the gap width x of such region, hence we can write:

$$F_m = F_m(i_d, i_q, x) \quad (24)$$

The values of the construction parameters k , F_{e0} , d , m and δ are provided in Table IV.

TABLE IV
PARAMETER VALUES FOR YOKE CONSTRUCTION DETAILS

Single mobile yoke mass, m	0.61 kg
Radius at mover rest position, R_0	47 mm
Spring constant, k	145 N/mm
Distance d	5 mm
Spring preload, F_{e0}	314 N

V. COMPUTATION OF MACHINE MODEL PARAMETERS

The motor model described in the previous Section includes some unknown functions that need to be determined based on design data. In particular, the unknowns are the flux linkages λ_d , λ_q given by (10) and the magnetic force F_m given by (24). All these quantities can be, in general, expressed as functions of stator currents i_d , i_q and of the gap x between mobile yokes and pole expansions. For the identification of such functions, a polynomial interpolation method based on a set of magneto-static FEA simulations is used next.

To achieve a complete characterization, FEA simulations are run for various discrete values of i_d and i_q currents and for different gap values x . From each simulation, the correspondent flux linkages λ_d , λ_q and magnetic force F_m are computed. Fortunately, the analysis is noticeably simplified by the fact that, based on FEA, d - q cross coupling phenomena [21] are found to be definitely negligible (cross-coupling inductances are in the order of 0.5% of d -axis one). This makes it possible to simplify (10) as follows:

$$\lambda_d = \lambda_d(i_d, x), \quad \lambda_q = \lambda_q(i_q, x) \quad (25)$$

A surface plot of the flux linkages identified by FEA is provided in Fig. 9.

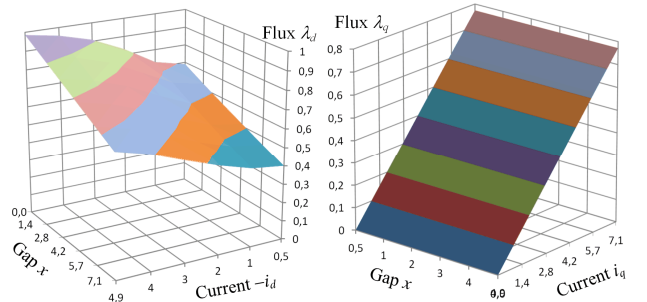


Fig. 9. d -axis and q -axis flux linkages as functions of i_d , i_q , x based on FEA. The gap x is in mm, i_d and i_q in A, λ_d and λ_q in wb.

From the inspection of Fig. 9 it clearly results that all the complications, associated with magnetic saturation and variable mobile yoke position, affect only the d axis. This can be intuitively justified looking at the field plots shown in Fig. 10.

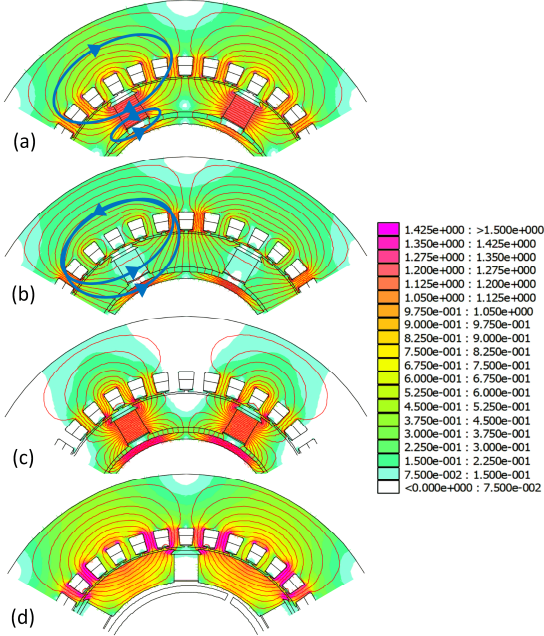


Fig. 10. Magneto-static FEA simulation results: (a) at no-load; (b) without permanent magnet and with a demagnetizing current $i_d = -8$ A; (c) with both permanent magnets and a demagnetizing current $i_d = -8$ A; with no permanent magnet and a q -axis current $i_q = -8$ A. In all cases $x = 2$ mm. The scale of flux density values is in teslas.

In particular, Fig. 10c shows that a q -axis current (although high) produces a magnetic flux that almost completely flows through the pole expansion (where magnetic saturation is negligible) without entering the mobile yoke. This explains why λ_q is practically insensitive to x and exhibits a linear growth low with respect to i_q , so that one can write:

$$\lambda_q = L_q i_q \quad (26)$$

where $L_q = 0.109$ H can be regarded as a constant q -axis inductance.

On the other side, the d -axis flux linkage λ_d appears to be a strongly nonlinear function of both i_d and x . The surface plot of λ_d is shown in Fig. 9 for negative (i.e. demagnetizing) values of i_d . In fact, magnetic saturation effects basically occur for negative i_d values only, while for positive (magnetizing ones), the variation of λ_d with i_d is essentially linear. This can be intuitively justified based on the field plots in Fig. 10a and Fig. 10b, which respectively show the flux paths due to permanent magnets only and to a d -axis demagnetizing current $i_d = -8$ A for the same gap $x = 2$ mm between mobile yokes and pole expansions. It can be seen that, while in the air gap and pole expansion (where saturation is negligible) the flux due to a negative i_d counteracts the one due to permanent magnets, conversely the two contributions (due to i_d and permanent magnets) have equal signs as regards the flux portion entering the mobile yokes. In other words, a demagnetizing (negative) i_d reduces the air-gap flux but increases the flux through

mobile yokes (where important magnetic saturation occurs). This can be easily seen from Fig. 10c where both permanent magnets and the stator current $i_d = -8$ A are present, resulting in a very weakened flux in the air gap and pole expansions and in a much stronger saturation of mobile yokes compared with Fig. 10a and Fig. 10b.

Although significantly nonlinear, the function $\lambda_d(i_d, x)$ exhibit a relatively smooth dependency on both i_d and x . In fact, using 2D polynomial interpolation techniques it is possible to approximate it with the simple doubly-quadratic expression below:

$$\lambda_d(i_d, x) = \begin{pmatrix} i_d^2 & i_d & 1 \end{pmatrix} \mathbf{M}_\lambda \begin{pmatrix} x^2 & x & 1 \end{pmatrix}^T \quad (27)$$

where \mathbf{M}_λ takes the following numerical value if i_d is expressed in amperes and x in millimeters:

$$\mathbf{M}_\lambda = \begin{pmatrix} -117 & 0.533 & 5.06 \times 10^{-4} \\ 2.47 \times 10^3 & -14.1 & -3.94 \times 10^{-2} \\ -1.01 \times 10^4 & 124 & 0.624 \end{pmatrix} \quad (28)$$

The approximation given by (27) leads to errors less than 3% with respect to the punctual values computed by FEA and, together with (26), offers the benefit of noticeably simplifying the computation of the flux derivatives that appear in (14), (15). Such derivatives can be in fact obtained symbolically as:

$$\partial \lambda_d / \partial i_q = \partial \lambda_q / \partial i_d = \partial \lambda_q / \partial x = 0$$

$$\partial \lambda_d / \partial i_d = \begin{pmatrix} 2i_d & 1 & 0 \end{pmatrix} \mathbf{M}_\lambda \begin{pmatrix} x^2 & x & 1 \end{pmatrix}^T \quad (29)$$

$$\partial \lambda_d / \partial x = \begin{pmatrix} i_d^2 & i_d & 1 \end{pmatrix} \mathbf{M}_\lambda \begin{pmatrix} 2x & 1 & 0 \end{pmatrix}^T$$

Regarding the computation of the magnetic force F_m , it has been already mentioned that, as clearly appears from Fig. 10c, a q -axis current gives rise to a magnetic flux that entirely flows through rotor pole expansions without entering mobile yokes. Since the magnetic force F_m is due to the flux between mobile yokes and pole expansions, it is then intuitive that i_q does not contribute to the magnetic force F_m . This is actually confirmed by FEA simulations and enables us to simplify (24) as follows:

$$F_m = F_m(i_d, x). \quad (30)$$

As done with flux linkages, the function $F_m(i_d, x)$ is identifying through a set of FEA simulations run for different discrete values of i_d and x . The resulting surface plot is given in Fig. 11.

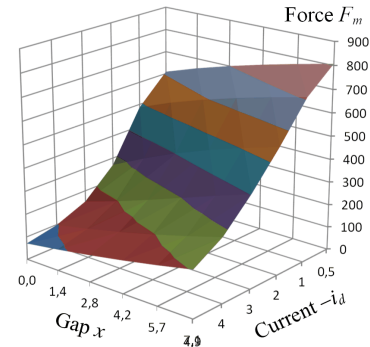


Fig. 11. Attractive magnetic force acting on a mobile yoke as a function of i_d and x , based on FEA simulations. The gap x is in mm, i_d in A and F_m in N.

In accordance with what has been observed above, the magnetic force, for a given gap x , grows if the demagnetizing (negative) i_d current increases. In fact, a demagnetizing (negative) i_d strengthens the flux (due to permanent magnets) between mobile yokes and pole expansions, as can be argued from Fig. 10a-c. For any given current i_d , F_m obviously decreases when the gap x grows due to the field intensity reduction in the region between yokes and pole expansions.

As done with flux linkages, also (30) can be approximated by 2D polynomial interpolation from FEA simulation results. However, in the case of F_m a satisfactory fitting (with errors below 3% with respect to FEA results) is achieved only if a cubic (instead of quadratic) interpolation is adopted to model the dependency on x . The polynomial approximated function is then defined in the form:

$$F_m(i_d, x) = \begin{pmatrix} i_d^2 & i_d & 1 \end{pmatrix} \mathbf{M}_F \begin{pmatrix} x^3 & x^2 & x & 1 \end{pmatrix} \quad (31)$$

where the constant matrix \mathbf{M}_F (supposing i_d expressed in amperes and x in millimeters) is:

$$\mathbf{M}_F = \begin{pmatrix} -0.2320 & 1.947 & -3.985 & 0.6970 \\ 2.207 & -21.30 & 51.79 & 11.85 \\ -3.331 & 60.30 & -359.7 & 779.9 \end{pmatrix} \quad (32)$$

VI. SIMULATION RESULTS AND MODEL EXPERIMENTAL ASSESSMENT

The IPM motor design described in the Section II and III, along its mathematical modeling described in Section IV and V, is validated through some dedicated tests on the machine laboratory prototype (Fig. 2-Fig. 4).

A. No-load analysis and testing

First of all, the prototype operation is analyzed and experimentally verified at no load. For this purpose, the machine, with open stator phases, is coupled to a pony motor (inverter-fed induction motor) and its speed is first ramped up from 0 to 2000 rpm and then reduced from 2000 to 0 rpm according to the acceleration and deceleration ramps shown in Fig. 12a.

Mobile yoke motion equation described in IV.D is integrated numerically using (30)-(32) to evaluate magnetic attractive force. Simulation results are shown in Fig. 12b-e in terms of the forces acting on each mobile yoke and in Fig. 12f in terms of how the gap width x evolves over time. It can be seen from Fig. 12e that, at low speeds (i.e. before instant $t=4$ s), the total force acting on the yoke is negative (i.e. oriented towards machine rotational axis) so that the yoke is retained in a detached position (Fig. 6a) and the gap width x is at its maximum value $x=5$ mm. As the speed increases, the centrifugal force grows so that the total force becomes positive and the yoke progressively displaces outwards causing the gap x to drop to zero (Fig. 6b). The process is seen not to be abrupt but to take approximately one second. As a consequence of yoke radial translation, the d -axis flux linkage λ_d , computed according to (27)-(28) for $i_d=0$, decays by around 40% (Fig. 12g). As a consequence of such flux weakening, in the rest of the acceleration process (i.e. between $t=5$ s and $t=10$ s), the motor voltage, computed through (16) and shown in Fig. 12h, grows along a new straight line which is lower than the initial one.

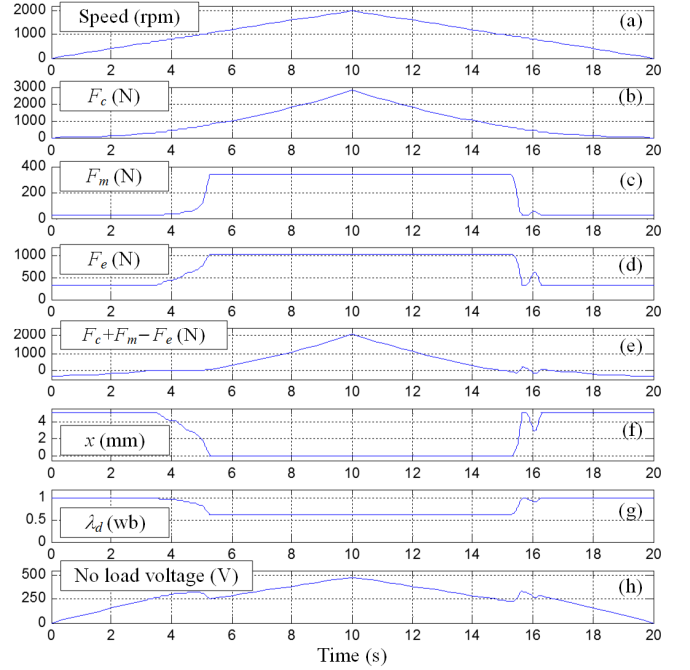


Fig. 12. Dynamic simulation of no-load machine acceleration from 0 to 2000 rpm followed by deceleration from 2000 to 0 rpm. The no load voltage is expressed in rms line-to-line volts.

During the deceleration (i.e. for $t>10$ s), the process is essentially reversed, although mobile yoke translation does not occur in an exactly specular way. In fact, when the speed ramps down, the high magnetic attraction force F_m would tend to keep yokes attached to pole expansions and the total force acting on yokes returns to be negative at around $t=15$ s. However, yoke transition occurs faster and slightly after $t=16$ s the initial air-gap $x=5$ mm is restored (Fig. 12f) as well as the original full motor flux (Fig. 12g).

Unfortunately, during acceleration and deceleration, neither the forces acting on mobile yokes nor their position can be accessed for measurement. However, it is possible to track machine open-circuit voltage, which bears evidence of all the non-observable phenomena taking place inside the machine rotor. The line-to-line voltage during speed ramps has been in fact recorded at a fixed sample rate together with motor speed. Measured voltage samples are plotted in Fig. 13 versus motor speed samples and, in the same plane, the voltage-versus-speed curves resulting from simulations are also drawn for comparison.

An overall good matching between experimental and simulation results can be observed. In particular, Fig. 13 shows how the mathematical model discussed in Sections IV and V is capable of predicting with sufficient accuracy the flux weakening phenomenon due to mobile yoke transition as well as the speed at which it takes place. Both measurements and simulation curves in Fig. 13 effectively highlight the slight hysteretic behavior of the system already observed above commenting on Fig. 12. The hysteretic behavior lies in the fact that mobile yoke transition occurs at slightly different speeds during acceleration and deceleration ramps, i.e. above 1000 rpm during acceleration and below 1000 rpm during deceleration. This phenomenon is strongly sensitive to how the mechanical flux weakening device is designed in terms of

spring elastic constant and preload and of mobile yoke mass. For example, the same hysteretic behavior has been reduced with respect to what reported in [19] by increasing each mobile yoke mass (through additional weights welded inside it) and by using springs with larger preload and elastic constant.

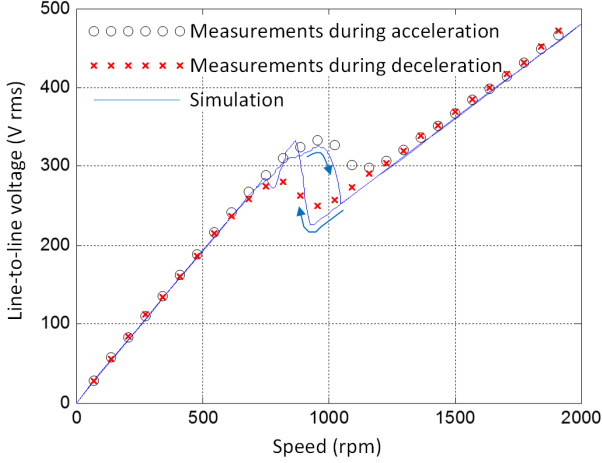


Fig. 13. Comparison between recorded and simulated motor voltage during acceleration and deceleration ramps between 0 and 2000 rpm.

B. Loaded operation analysis and testing

As a further analysis and testing activity, the IPM motor operation in loaded conditions is studied through the proposed model and experimentally assessed on the prototype. For this purpose, the motor is loaded by a converter-fed induction machine (which operates in regenerating mode) and supplied by a synchronous generator with manually-controllable excitation. By acting on the supply generator excitation and on the reference torque of the induction machine load, it is possible to have the IPM motor under test operate at steady-state working points which belong to the voltage-vs-speed and torque-vs-speed characteristics shown in Fig. 14a.

The constant-power region, which coincides with the flux weakening region [5], is entered above 1000 rpm, which is close to the speed around which the mechanical flux weakening of the motor occurs (Section VI.A).

In order to assess the benefits of the proposed mechanical flux weakening device with respect to the conventional spoke-type IPM motor design, tests are repeated in two conditions, namely with the mobile yokes normally operating (Sections II and III) and with the mobile yokes mechanically blocked in their rest (low speed) position (Fig. 6a). This latter situation reproduces the case of a conventional IPM motor.

Machine performance under the imposed torque and voltage versus speed profiles is studied through the mathematical model described in Sections IV and V; simulation results are illustrated in Fig. 14b-e in terms of i_d , i_q and total stator current amplitudes and in terms of power factor. In particular, total current and power factor values are compared to measured ones in Fig. 14d and Fig. 14e. The comparison shows a good accordance between theoretical predictions and experimental data for both machine configurations (with either blocked or mobile rotor yokes).

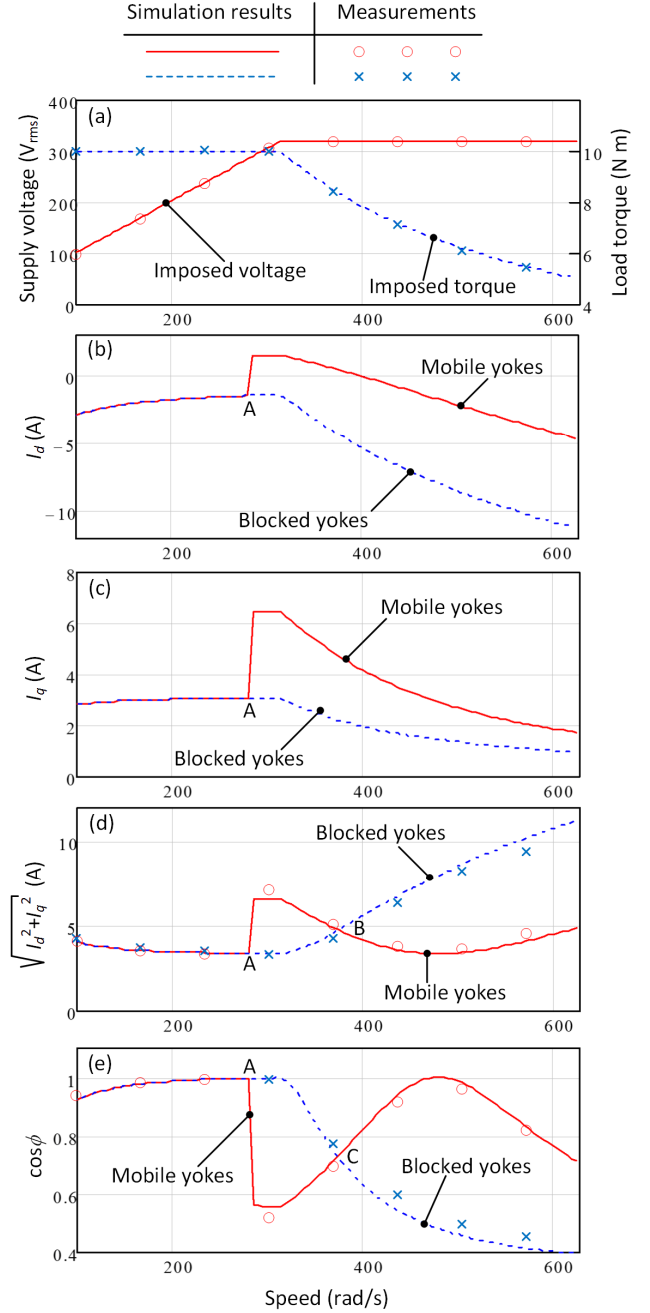


Fig. 14. Simulation and measurement results for motor operation with imposed voltage and torque profiles over 0-2000 rpm speed-range.

Fig. 14 effectively highlights the usefulness of the proposed mechanical flux weakening device with respect to the conventional IPM motor.

The two motor configurations obviously behave in the same way on the left of the point (indicated with letter A in Fig. 14) at which mobile yokes activate. In correspondence of point A, the current i_d becomes positive in the mobile-yoke motor arrangement (Fig. 14b). In fact, a positive (magnetizing) i_d current is required to compensate for the flux loss due to mobile yoke activation. When the flux weakening starts and for higher speeds, however, the i_d current reduces and returns to be negative, remaining significantly lower in magnitude compared to the blocked-yoke case (Fig. 14b). This is to be

regarded as a gain, since the proposed design requires lower demagnetizing current (i_d) to follow the imposed voltage-versus-speed profile.

On the other side, Fig. 14c shows that, to the right of point A, the q -axis current i_q is higher in the mobile-yoke arrangement than in the conventional (blocked-yoke) one due to the reduced rotor flux. This is to be obviously regarded as a drawback, or, in other words, as the toll to be paid for the reduction in machine flux.

The overall impact in terms of absorbed current is visible from Fig. 14d, where the total phase current is plotted as a function of the speed. Fig. 14d shows that, within the speed range included between points A and B, the total current is actually higher for the proposed design than for the conventional IPM motor as a consequence of the larger i_q current required (Fig. 14c). Nevertheless, to the right of point B, the benefit of a reduced i_d current (Fig. 14b) prevails over the drawback of a larger i_q current (Fig. 14c) so that the total current absorbed by the proposed IPM motor with mobile yokes is significantly lower at high speeds than for the traditional IPM one.

A similar phenomenon can be observed from Fig. 14e in terms of power factor. Between points A and C the power factor is higher with blocked yokes than with mobile ones. Instead, at higher speeds (to the right of point C), the power factor drops to extremely low values in the conventional IPM motor case while it keeps relatively high in the proposed configuration with mobile rotor yokes.

In conclusion, one can state that the proposed flux weakening device is certainly advantageous if the speed range of the machine needs to be extended and the benefits are particularly important at high speeds. Such benefits can be summarized as follows: reduced total current absorption and, hence, reduced inverter sizing requirement; reduced copper losses and consequently improved efficiency.

VII. CONCLUSION

In this paper, a novel spoke-type IPM motor design for improved flux weakening capabilities has been described. The proposed design consists of equipping the machine with mobile yokes placed between rotor pole expansions and the shaft. At low speeds mobile yokes are retained close to the shaft by means of springs while, at high speeds, they displace radially due to centrifugal force up to touching rotor pole expansions. This increases permanent-magnet leakage fields and thereby reduces the air-gap flux without the need for demagnetizing current injection from the inverter. The proposed design has been investigated in this paper by means of a mathematical dynamic model, accounting for magnetic saturation effects. Model parameters have been identified through a set for magneto-static FEA simulations. Tests on a laboratory prototype have been presented to show the effectiveness of the proposed solution in enhancing motor performance at high speeds in terms of reduced absorbed current and copper losses with respect to a conventional IPM motor design. Experimental results have been also used to validate the electromechanical model proposed to study the new IPM machine topology.

ACKNOWLEDGEMENT

The work reported in this paper has been funded by Regione Friuli Venezia Giulia under Regional Law 14/2010.

REFERENCES

- [1] Ping-Yi Lin, Yen-Shin Lai, "Voltage Control Technique for the Extension of DC-Link Voltage Utilization of Finite-Speed SPMSM Drives", *IEEE Transactions on Industrial Electronics*, vol.59, no.9, pp.3392-3402, Sept. 2012.
- [2] D. Y. Kim, J. K. Nam, G. H. Jang, "Reduction of Magnetically Induced Vibration of a Spoke-Type IPM Motor Using Magnetomechanical Coupled Analysis and Optimization", *IEEE Transactions on Magnetics*, vol. 49, no. 9, Sept. 2013, pp. 5097-5105.
- [3] D.G. Dorrell, A.M. Knight, L. Evans, M. Popescu, "Analysis and design techniques applied to hybrid vehicle drive machines—Assessment of alternative IPM and induction motor topologies", *IEEE Transactions on Industrial Electronics*, vol.59, no.10, pp. 3690-3699, Oct. 2012.
- [4] Aimeng Wang, Yihua Jia, W.L. Soong, "Comparison of Five Topologies for an Interior Permanent-Magnet Machine for a Hybrid Electric Vehicle", *IEEE Transactions on Magnetics*, vol. 47, no. 10, Oct. 2011, pp. 3606-3609.
- [5] Ki-Chan Kim, "A Novel Magnetic Flux Weakening Method of Permanent Magnet Synchronous Motor for Electric Vehicles", *IEEE Transactions on Magnetics*, vol. 48, no. 11, Nov. 2012, pp. 4042-4045.
- [6] D. G. Dorrell, M. F. Hsieh, and A. M. Knight, "Alternative rotor designs for high performance brushless permanent magnet machines for hybrid electric vehicles," *IEEE Transactions on Magnetics*, vol. 48, no. 2, Feb. 2012, pp. 835–838.
- [7] Sung-II Kim, Jinwoo Cho, Sunghyuk Park, Taesang Park, Seongtaek Lim, "Characteristics Comparison of a Conventional and Modified Spoke-Type Ferrite Magnet Motor for Traction Drives of Low-Speed Electric Vehicles", *IEEE Transactions on Industry Applications*, vol. 49, no. 6, Nov./Dec. 2013, pp. 2516-2523.
- [8] J. Aubry, H. Ben Ahmed, B. Multon, "Sizing Optimization Methodology of a Surface Permanent Magnet Machine-Converter System Over a Torque-Speed Operating Profile: Application to a Wave Energy Converter", *IEEE Transactions on Industrial Electronics*, vol.59, no.5, May 2012, pp.2116-2125.
- [9] C. Jo, J.-Y. Seol, and I.-J. Ha, "Flux-weakening control of IPM motors with significant effect of magnetic saturation and stator resistance", *IEEE Transactions on Industrial Electronics*, vol.55, no.3, Mar. 2008, pp. 1330-1340.
- [10] R. Menis, M. Mezzarobba, A. Tassarolo, "A survey of mechanical and electromagnetic design techniques for permanent-magnet motor flux-weakening enhancement", *Electrical Systems for Aircraft, Railway and Ship Propulsion (ESARS)*, 2012, 16-18 Oct. 2012.
- [11] H. Woehl-Bruhn, W.-R. Canders, N. Domann, "Classification of field-weakening solutions and novel PM machine with adjustable excitation", *2010 XIX International Conference on Electrical Machines (ICEM)*, 6-8 Sept. 2010.
- [12] Baoquan Kou, Chunyan Li, Shukang Cheng, "Flux-Weakening-Characteristic Analysis of a New Permanent-Magnet Synchronous Motor Used for Electric Vehicles", *IEEE Transactions on Plasma Science*, vol.39, no.1, Jan. 2011, pp.511-515.
- [13] G. Krebs, L. Daniel, "Giant Magnetostrictive Materials for Field Weakening: A Modeling Approach", *IEEE Transactions on Magnetics*, vol. 48, no. 9, Sept. 2012, pp. 2488-2494.
- [14] L. Ma, M. Sanada, S. Morimoto, Y. Takeda, N. Matsui, "High Efficiency Adjustable Speed Control of IPMSM with Variable Permanent Magnet Flux Linkage", *34th IEEE Industry Applications Society Annual Meeting*, 3-7 Oct. 1999, vol.2, pp.881-887.
- [15] K. Baoquan, L. Chunyan, C. Shukang, "A New Flux Weakening Method of Permanent Magnet Synchronous Machine," *8th International Conference on Electrical Machines and Systems, ICEMS 2005*, 27-29 Sept. 2005, vol.1, pp. 500-503.
- [16] Mizanoor Rahman Mohammad, Kyung-Tae Kim, Jin Hur, "Design and Analysis of a Spoke Type Motor With Segmented Pushing Permanent Magnet for Concentrating Air-Gap Flux Density", *IEEE Transactions on Magnetics*, vol. 49, no. 5, May 2013, pp. 2397-2400.
- [17] Mohammad Mizanoor Rahman, Kyung-Tae Kim, Jin Hur, "Design and Optimization of Neodymium-Free Spoke-Type Motor With Segmented

- Wing-Shaped PM”, *IEEE Transactions on Magnetics*, vol. 50, no. 2, Feb. 2014, paper ID: 021404.
- [18] Hyung-Wook Kim, Kyung-Tea Kim, Yung-Sik Jo, Jin Hur, “Optimization Methods of Torque Density for Developing the Neodymium Free Spoke-Type BLDC Motor”, *IEEE Transactions on Magnetics*, vol. 49, no. 5, May 2013, pp. 2173-2176.
- [19] A. Tassarolo, M. Mezzarobba, R. Menis, “A New Rotor Design for Flux Weakening Capability Improvement in Spoke-Type Interior-Permanent-Magnet Synchronous Machines”, *International Conference and Exhibition on Ecological Vehicles and Renewable Energies, EVER 2014*, Montecarlo, Monaco, 25-27 March 2014, paper ID ever14-116.
- [20] C. Bassi, D. Giulivo, A. Tassarolo, “Time-Stepping Finite-Element Analysis of a 14 MVA Salient-Pole Shipboard Alternator for Different Damper Winding Design Solutions”, *IEEE Transactions on Industrial Electronics*, vol. 59, no. 6, 2012, pp. 2524-2535.
- [21] G. Qi, J.T. Chen, Z.Q. Zhu, D. Howe, L.B. Zhou, C.L. Gu, “Influence of Skew and Cross-Coupling on Flux-Weakening Performance of Permanent-Magnet Brushless AC Machines”, *IEEE Transactions on Magnetics*, vol. 45, no. 5, May 2009, pp. 2110-2117.
- [22] R. Menis, M. Mezzarobba, A. Tassarolo, “A survey of mechanical and electromagnetic design techniques for permanent-magnet motor flux-weakening enhancement”, *Electrical Systems for Aircraft, Railway and Ship Propulsion (ESARS), 2012*, 16-18 Oct. 2012.
- [23] K.I. Laskaris, A.G. Kladas, “Internal Permanent Magnet Motor Design for Electric Vehicle Drive”, *IEEE Transactions on Industrial Electronics*, vol.57, no.1, pp.138-145, Jan. 2010.
- [24] A. Tassarolo, M. Mezzarobba, R. Menis, “A novel interior permanent magnet motor design with a self-activated flux-weakening device for automotive applications”, *2012 XXth International Conference on Electrical Machines (ICEM)*, pp.2603-2609, 2-5 Sept. 2012.
- [25] Shuangxia Niu, S.L. Ho, W.N. Fu, Jianguo Zhu, “Eddy Current Reduction in High-Speed Machines and Eddy Current Loss Analysis With Multislice Time-Stepping Finite-Element Method”, *IEEE Transactions on Magnetics*, vol.48, no.2, pp.1007-1010, Feb. 2012.
- [26] Zhuang Xu, “An adaptive sliding stator flux observer for a direct-torque-controlled IPM synchronous motor drive”, *IEEE Transactions on Industrial Electronics*, vol.54, no.5, 2007, pp. 2398-2406.

Alberto Tassarolo (M’06) received his Laurea and Ph.D. Degrees in Electrical Engineering from the University of Trieste and Padova in 2000 and 2011, respectively. Since 2006 he served as an electric motor and generator design engineer with Nidec-ASI (formerly Ansaldo Sistemi Industriali). Presently, he is an assistant professor at the Engineering and Architecture Dept. of the University of Trieste where he teaches the course of Electric Machine Design. His main research interests are in electric machine and drive modeling, analysis and design optimization, a field in which he has authored more than 100 international papers. He leads several research and development projects in cooperation with electric machine manufacturers and final users. He serves as an Editor for the IEEE Transactions on Energy Conversion. He is a member of IEEE and of various IEEE Societies (PES, IAS, PELS, IES, Magnetics and Reliability Societies). He is a registered professional engineer in Italy.

Mario Mezzarobba received his Laurea Degree in Electrical Engineering from the University of Trieste, Italy, in 2008 and his Ph.D. degrees in Electrical Engineering from the University of Padova, Italy, in 2012. Since 2008, he has actively taken part in various consultancy activities for the dimensioning and design of electromechanical components and systems. Currently, he serves as a research assistant at the Engineering and Architecture Department of the University of Trieste, Italy. His main research interests are in the field of electric machine design and optimization.

Roberto Menis (S’76–M’92) was born in Osoppo, Italy. He received his Laurea degree in Electronic Engineering from the University of Trieste, Trieste, Italy, in 1982. From 1982 to 1984, he was a member of the Technical Staff of an aeronautic industrial company. In 1984, he joined the University of Trieste, where he is currently an Associate Professor of Electric Drives. His research interests are in the field of electric machines and drives and include: modeling, identification and control of AC machines, control of synchronous generators for diesel-alternator groups and design of drives for industrial applications.